



**HAL**  
open science

## Experimental investigation of galling occurrence in sliding contact under high pressure of a manganese phosphate versus steel interface: Comparison of two greases

Pauline Faura, Siegfried Fouvry, Clotilde Minfray, Pauline Ronfard, Alberto Benitez, Xavier Mencaglia, Jules Galipaud

### ► To cite this version:

Pauline Faura, Siegfried Fouvry, Clotilde Minfray, Pauline Ronfard, Alberto Benitez, et al.. Experimental investigation of galling occurrence in sliding contact under high pressure of a manganese phosphate versus steel interface: Comparison of two greases. *Wear*, 2023, 524-525, pp.204820. 10.1016/j.wear.2023.204820 . hal-04137716

**HAL Id: hal-04137716**

**<https://hal.science/hal-04137716v1>**

Submitted on 26 Nov 2023

**HAL** is a multi-disciplinary open access archive for the deposit and dissemination of scientific research documents, whether they are published or not. The documents may come from teaching and research institutions in France or abroad, or from public or private research centers.

L'archive ouverte pluridisciplinaire **HAL**, est destinée au dépôt et à la diffusion de documents scientifiques de niveau recherche, publiés ou non, émanant des établissements d'enseignement et de recherche français ou étrangers, des laboratoires publics ou privés.

P. Faura, S. Fouvry, C. Minfray, P. Ronfard, A. Benitez, X. Mencaglia, J. Galipaud,

Experimental investigation of galling occurrence in sliding contact under high pressure of a manganese phosphate versus steel interface: Comparison of two greases, *Wear* 524-525 (2023) 204820  
(<https://doi.org/10.1016/j.wear.2023.204820>) < hal-04137716>

## **Experimental investigation of galling occurrence in sliding contact under high pressure of a manganese phosphate versus steel interface: comparison of two greases**

**Pauline Faura<sup>1,2)\*</sup>, Siegfried Fouvry<sup>1)</sup>, Clotilde Minfray<sup>1)</sup>, Pauline Ronfard<sup>2)</sup>, Alberto Benitez<sup>3)</sup>, Xavier Mencaglia<sup>2)</sup>, Jules Galipaud<sup>1)</sup>**

<sup>1)</sup>LTDS, Ecole Centrale de Lyon, Ecully, France

<sup>2)</sup>Vallourec Research Center, Aulnoye-Aymeries, France

<sup>3)</sup>Davricourt – Lille, Lille, France

\*Corresponding author: pauline.faura@ec-lyon.fr

### Abstract

In OCTG (Oil Country Tubular Goods) field, surface treatments and greases are used to make connections reliable by avoiding galling in metal-metal contacts. This study compares the anti-galling performances and wear behavior of two tribo-systems: steel versus manganese phosphate coated steel contact tested with two different greases. The damage scenario and the kinetics of the involved tribological phenomena will be investigated thanks to a test based on the ASTM G196 standard and appropriate surface analyses. A rotational oscillatory movement is applied on two cylindrical samples under static normal loads. Friction coefficient is computed using torque-sensor records. Counterparts are made of carbon steel of yield strength 550 MPa. One has been subjected to a manganese phosphate treatment to generate a protective layer of few microns thick. The other counterpart is used as machined. Two different industrial greases with anti-wear and extreme pressure additives are tested. Results showed a significant difference of tribological behavior between both greases. XPS analyses are done to understand the composition of the interfacial materials. The protective mechanisms of both greases are compared. Pb-containing grease allows the instantaneous formation of a protective layer whereas Pb-free grease forms a thin and durable protective layer after quite long running-in phase. Manganese phosphate layer participate in the protective layer formation.

### 1) Introduction

Pipe strings for oil and gas production are composed of around 13-meters-long tubes screwed to each other [1] as illustrated in Figure 1. Strings endure severe loadings as they are installed in deep wells and during production phase [2]. Tubes and connections between the tubes must resist these loadings while ensuring sealability. Sealability is achieved during installation phase while the tube is screwed to one other thanks to the metal-to-metal (MTM) seal designed in the connection. During the make-up of the connection, high contact pressure is applied on the MTM seal such that the junction is gas-tight at the end of tube installation [3]. During their lifetime, tubes may be disassembled and re-assembled, while keeping their initial performance. The repetitive sliding under high pressure at the MTM seal can generate wear and even galling of the surfaces. A galled seal after make-up of a connection is shown in Figure 1.

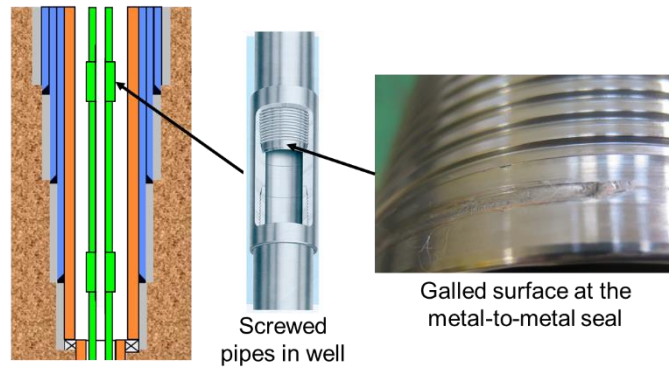


Figure 1 Illustration of the galling phenomenon in a screwed assembly of steel tubing

Galling is defined as a surface damage arising between surface sliding solids distinguished by macroscopic, usually localized, roughening and creation of protrusions above the original surface [4]. It may involve non-uniform material transfer and/or plastic flow on both macroscopic and microscopic scales [5]. To avoid galling appearance in the seal, surface treatments are applied on the connections. One commonly utilized is a manganese phosphate treatment with the application of grease before the tube is screwed. Tribological behavior and anti-galling performance of manganese phosphate with grease have been studied by several authors [6–10]. Wear mechanism of phosphating treatment in a lubricated sliding contact is summarized by Ernens *et al.* [8]. Phosphate layer breaks at the top of the tips of phosphate grains and the debris are mixed with lubricant -grease oil in that case - under sliding loading. This forms a protective tribofilm at the top of the phosphating treatment. This protective layer is progressively eliminated by shear stress allowing metal-to-metal contact and eventually galling.

Several tests are used to capture galling events in literature. One of them is available in the norm ASTM G196 [4]. Two cylindrical specimens are put in contact with the ends mated under a selected contact pressure. One specimen is rotated around its axis and the other is held fixed. The results of the experimentations provide the rate of galling occurrences for the given loading conditions and allow a preliminary material ranking [11]. In OCTG field, a pin-and-box rig has been developed by Ertas *et al.* reproducing accurately the contact conditions found in a connection [12]. This test machine can be used to analyze friction behavior and galling resistance of different materials [13,14].

The objective of this work is to study the anti-galling performance and tribological behavior of a steel contact treated with manganese phosphate and two different greases. A specific test inspired by the ASTM G196 is used. Wear mechanism with two commercial greases containing solid additives used in OCTG connections are investigated under similar sliding conditions than the industrial conditions.

## II) Experimental set-up

### Test machine

A test bench based on the ASTM G196 principle has been set up using a hydraulic axial-torsional machine (Figure 2a). Two cylindrical specimens are put in contact by their section (Figure 2b). One specimen is mounted in the upper holder which is static. The other specimen is mounted in the bottom holder which is clamped in the actuator applying normal force and rotation. The test system ensures axial alignment between both samples. A truncated conical shape has been designed on the upper sample surface such that the surface of contact is ring-shaped illustrated in Figure 1c. The resulting contact area is about 106.8 mm<sup>2</sup>. This geometry is representative of the real contact geometry size and allows a contact pressure control even in case of wear. However, in the real application, contact geometries may differ depending on the connection type: truncated conical shape exists as well as curved profiles with different curvature radius.

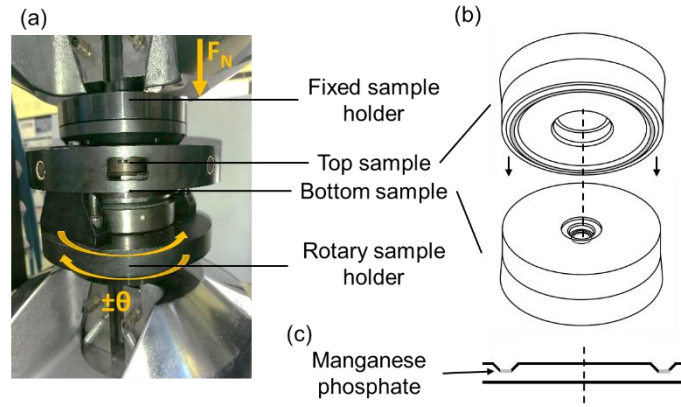


Figure 2 (a) Galling tester assembly, (b) shape of the specimens, (c) shape of the contact

### Test procedure

Tests were performed at constant frequency and contact pressure. Both greases have been tested at three pressure levels (400 MPa, 650 MPa, 900 MPa) corresponding to three normal forces (43k N, 70 kN, 96 kN). The range of pressure represents the contact pressure applied on seal at the end of the make-up for several sizes of connections. Alternated rotation is applied with an amplitude of +/- 25° on the bottom sample. The alternated rotation allows to achieve high sliding distances necessary to observed galling appearance. Amplitude and frequency were chosen to apply a similar linear sliding speed than the linear speed applied on the seal during the connection make-up. In one cycle, a sliding distance of 29.7 mm is done. The maximum torque reached during a cycle is used to compute the friction coefficient of the cycle. For each pressure level, three repetitions were made letting the friction coefficient grow until 0.16 to ensure that galling has happened with no possible recovery. Between two and four interrupted tests were performed in each configuration to learn about the wear scenario detailed in Table 1.

Table 1 Loading conditions and interruption conditions of the tests

Grease	Frequency Hz	Amplitude °	Pressure MPa
BOL	0.4	± 25	400 – 650 – 900
API	0.4	± 25	400 – 650 – 900

Two characteristic values were used to compare grease performance; they are extracted from the friction curve as illustrated in Figure 3. The sliding distance necessary to reach a friction coefficient of 0.16  $N_c$  is used to compare the endurance of each configuration before incipient galling. Indeed, previous observations with the same carbon steel have shown that the galling phenomenon has already took place in the interface when the friction level reaches 0.16 [15]. The friction level at half of the critical number of cycles  $N_c$  is used to capture the friction level reached by the tribo-system during the plateau of the friction coefficient. The lubricated phase of the test starts after the running-in phase (where friction may be high) and ends right before the final COF increase.

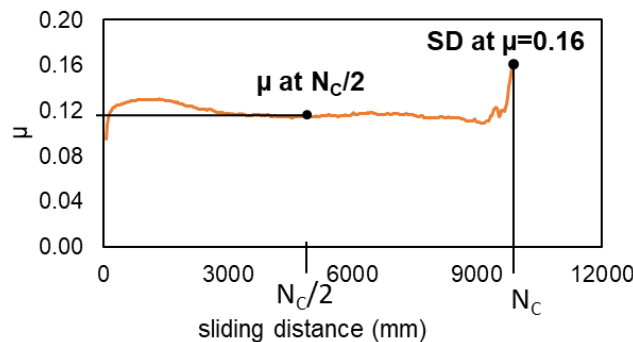


Figure 3 Characteristic values  $\mu$  at  $N_c/2$  and  $N_c$  (at  $\mu=0.16$ ) extracted from the friction curve

Surface analyses are made using surface profiler, SEM and XPS equipment. Surface topography is obtained using the vertical scanning interferometry (VSI) measurement mode of Wyko NT9800/9300 surface profiler. SEM observations are done using TESCAN Mira 3 FEG SEM. XPS analyses are made using an ULVAC – PHI Versaprobe III Spectrometer equipped with a monochromatized AlK $\alpha$  X – ray source (1486.6 eV). Spot size used is 200  $\mu$ m. Charge compensation system is used to compensate the charging effect. Additional charge correction was done by fixing the C1s peak (C-C bond) at 284.8 eV. Survey spectra were recorded with a pass energy of 224 eV in the range 0 – 1100 eV. High resolution spectra were obtained with a range of 20 eV and a pass energy of 13 eV. The peaks are fitted with a Shirley background and the quantification is done with following sensitivity factors [16]. All the peaks were fitted and analyzed using CasaXPS software.

### Surface treatment

The bulk specimens are made of carbon steel with a composition detailed in Table 2. A specific heat treatment including a water quench followed by a tempering treatment is applied leading to a 550 MPa yield strength [17].

Table 2 Steel composition (mass fraction)

	C	Mn	Ni	Cu	P	S	Si
% max	0.43	1.90	0.25	0.35	0.030	0.030	0.45

Upper specimen is coated using a manganese phosphate treatment further identified as Mn-P. To be phosphatized, specimens are dropped in a bath of aqueous solution containing phosphoric acid and manganese primary phosphate. The surface of the steel is attacked by the acid then phosphate grains initiate at the surface and grow leading to a complete rough layer. Figure 4a shows an SEM observation of the Mn-P used in this study, the size of the grain is about 2-3  $\mu$ m. To set the initial composition of the surface of the Mn-P samples, XPS analyses have been done (Figure 4b, c) after cleaning in ultrasonic bath with successive solvents (heptane, isopropanol and acetone). The XPS analyses show the presence of manganese, phosphorus and oxygen which is consistent with the expected composition of the Mn-P layer. Carbon peak is present due to extreme surface contamination. Calcium and small amount of zinc and cobalt are found attributed to the contamination during the phosphatizing process. Peaks assignation of the high-resolution spectra of the different elements is done in Table 3.

Table 3 Pic assignation of the high-resolution spectra from XPS analyses of Mn-P layer

	Exp. values on Mn-P	Chiba et al., 2000 [18]	Cai et al., 2018 [19]	Guo et al., 2021 [20]
<b>O 1s</b>				
H <sub>2</sub> O, POP	<b>533.2</b>	532-533		
O-Mn, PO <sub>4</sub> <sup>3-</sup> , OH	<b>530.7</b>			530.91
HPO <sub>4</sub> <sup>2-</sup>	<b>531.9</b>			532.19
<b>P 2p</b>	<b>133.2</b>			
<b>Mn 2p3/2</b>				
Mn <sup>2+</sup>	<b>641.3</b>		640.5	640.95
Mn <sup>4+</sup> , oxyde	<b>643</b>		642.5	642.92
Sat 2p3/2	<b>645.8</b>		647	645.7

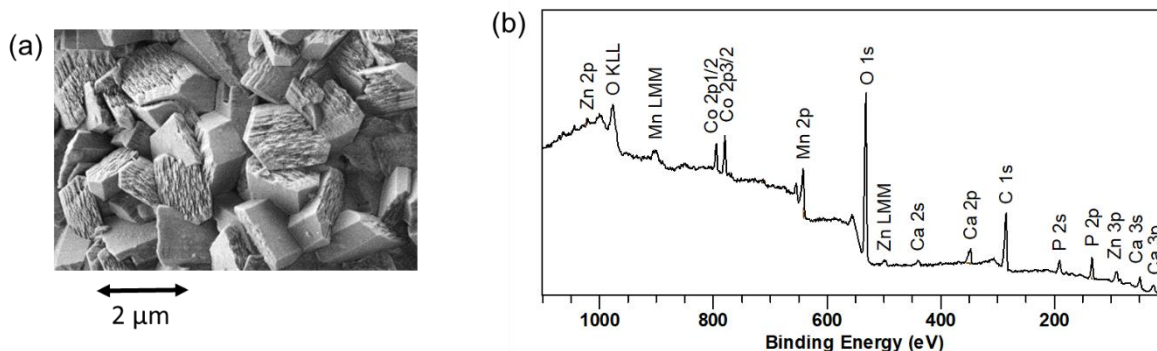


Figure 4 (a) SEM observation of the Mn-P layer, (b) XPS spectra of the Mn-P layer

## Greases

The commercial greases used for the tests are provided by Bestolife<sup>®</sup>, these greases are commonly used in the OCTG field. Both are following the specifications of the API norm 5A3 [21]. One is following the composition proposed in the norm API, called API modified thread compounds and contains metallic additives (particularly lead particles), it will be identified as “API”. The second one is a heavy metal-free grease and will be identified as “BOL”. Table 4 gathers the detailed composition of both greases. Grease is applied in the same way for each test. A brush is used to deposit the grease on the sliding surface, and then the extra-material is removed using a jig. Procedure is designed to reproduce the grease application in the industrial context where a 0.1 mm thick layer is needed.

*Table 4 Composition of both commercial greases API and BOL*

Commercial name	Bestolife <sup>®</sup> API modified	Bestolife <sup>®</sup> 4010 <sup>®</sup> NM
Abbreviation in paper	API	BOL
Base oil	Petroleum	Synthetic
Thickeners	Lithium soap	Calcium complexes
Additives	Lead, graphite, zinc, copper metal powder, talc, quartz	Graphite, talc, titanium dioxide

### III) Results

#### Friction

Friction curves versus sliding distance are shown in Figure 5. The shape of the curve and the friction level are strongly dependent of the type of the grease. For API, the friction is low at the beginning of the test and increases slowly. After some tens of cycles, friction starts to increase faster and faster until reaching a 0.16 friction coefficient. In case of BOL, friction coefficient increases fastly at the beginning of the test until reaching a coefficient of friction around 0.1 depending on the pressure level. Then, the friction coefficient decreases slowly during few hundreds of cycles also depending on the pressure level. At the end, a sharp increase in the friction level indicates the end of the test in few cycles. Friction coefficient at the half of the critical cycle is decreasing with the increase of charge in the same way for both greases. Friction level at  $N_c/2$  is always lower for the grease API (around 0.08) than BOL (around 0.12). For API, the sliding distance before galling apparition is stable with pressure whereas for BOL, the endurance decreases. The scattering seen on Figure 5d is relatively high. When looking at the curves, it appears that the main part of the tests is very similar for each repetition, the difference lies in the appearance of the final sharp increase – galling occurrence and propagation. For clarity reasons, only one curve for each test condition is plotted on Figure 5 a & b to show the morphology of friction curves, the scattering being represented Figure 5 c & d. Wear analyses presented later (Figure 6) have been done on different couples which may have lasted longer or shorter than tests with the curves plotted.

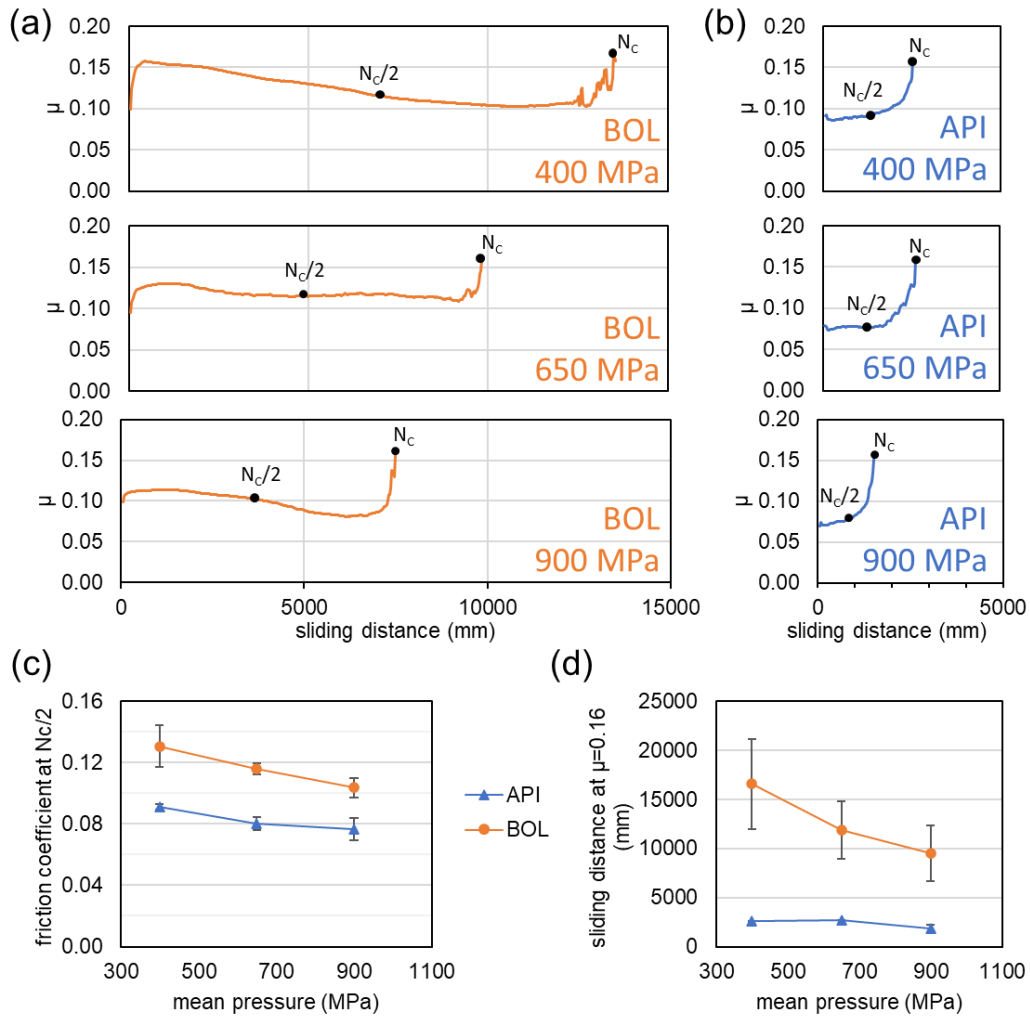


Figure 5 (a) Friction coefficient versus sliding distance at contact pressures of 400 MPa, 650 MPa and 900 MPa for (a) BOL and (b) API, (c) friction coefficient at  $N_c/2$  for BOL and API versus contact pressure, (d) sliding distance  $N_c$  at  $\mu=0.16$  for BOL and API versus contact pressure ( $f=0.4$  Hz,  $\vartheta^*=\pm 25^\circ$ ,  $D=\pm 7.2$  mm)

## Wear

Surface analyses have been done after a careful cleaning of the specimens. Specimens were cleaned up using an ultrasonic bath and different solvents successively (heptane, isopropanol, and acetone). Topographic line profiles have been done on the worn tracks of the bottom specimen for each interrupted test (Figure 6a, b).

For the tests done with the BOL, wear is evenly distributed along the track's width and the track is smooth before galling onset. Wear depth increases with the sliding distance. Once galling has been initiated (sliding distance of 14 000 mm), surface is more disturbed with deep grooves and a significant increase in roughness parameter  $R_a$ .

For the tests done with the API, wear is uniformly distributed at the really beginning of the test. The track is heterogeneous as can be seen on SEM observation (Figure 6b). At the middle of the test, track is still heterogeneous and wear profile has been refilled at some places with thick "patches" of the third-body layer. At the galling onset, wear profile is disturbed and  $R_a$  increases similarly as the BOL grease.

Negative wear volume has been extracted from the 2D profiles, results for BOL and API at the medium pressure 650 MPa are shown in Figure 6c. Again, two different behaviors can be observed for each grease. In case of BOL tests, wear volume increases instantaneously as test begins up to  $0.4 \text{ mm}^3$  for medium pressure 650 MPa ( $0.16 \text{ mm}^3$  at 400 MPa and  $1 \text{ mm}^3$  at 900 MPa). Once running-in period is over, wear increases slowly during the test. In the presence of API, wear volume increases quite fast all the test duration long reaching  $0.3 \text{ mm}^3$  at medium pressure ( $1.5 \text{ mm}^3$  at 900 MPa).

## Interfacial materials

SEM and EDS analyses are shown Figure 7a for BOL and Figure 8a for API. Analyses were made on the top and bottom samples for each interrupted test. XPS analyses were made for the medium sliding distance on the top and the bottom in and out of the wear tracks. Resulting general spectra are shown in Figure 7b for BOL and Figure 8b for API. This way, XPS analyses show extreme surface composition (detailed in Table 5) right after application of the grease (XPS analyses outside the contact) and after a sliding distance of  $N_c/2$  (5000 mm for BOL and 900 mm for API – XPS analyses inside wear tracks). Elements found on each sample by EDS and XPS are gathered in Table 6 with the origin of each element in the interface.

For the BOL tests, EDS analysis (Figure 7a) suggests that elements of Mn-P and of the grease (Ca) are present in the interface early in the test (900 mm) and get well distributed all over the contact surface later during the lubricated phase (at 5000 mm). Mn-P and grease elements are ejected from the contact once galling has initiated starting from the edge of the track.

It is different in case of API. Mn-P layer is quickly worn out from substrate at the edge of the tracks and at different zones in the center of the track (Figure 8a). Grease elements are dispersed on the top sample. Lead has stuck on the bottom sample on almost the whole surface (some pieces are lacking). In both case, galling initiates (after critical cycle  $N_c$  is reached) at the edge of the contact first and then extends to the center as Mn-P and grease are ejected.

*Table 5 Proportion of elements detected by XPS on extreme surface of Mn-P layer, BOL samples and API samples (in the samples name, "Top" means "top sample", "bot" means "bottom sample", "in" means "in the wear track" and "out", "out of the track")*

Sample	C At %	O At %	P At %	Mn At %	Fe At %	Ca At %	Mg At %	Zn At %	Pb At %	Cu At %	Co At %
Mn-P	35.46	42.15	5.62	4.74	0.3	1.79	7.42	0.26	-	-	2.26
Top BOL out - A	48.81	37.78	4.76	3.25	0.46	2.32	1.92	0.4	-	-	0.3
Top BOL in - B	63.6	30.56	0.71	1.23	0.1	3.72	-	-	-	-	0.08
Bot BOL out - C	74.21	18.64	-	-	1.18	1.25	-	-	-	-	4.72
Bot BOL in - D	68.4	19.49	0.5	0.3	-	1.97	5.55	-	-	-	3.79
Top API out - E	46.49	34.47	5.98	-	0.58	1.45	7.99	0.65	0.81	-	1.46
Top API in - F	62.72	26.14	3.84	-	-	-	-	1.64	4.49	0.49	0.68
Bot API out - G	50.6	36.17	-	-	6.81	0.68	-	0.57	1.21	-	3.5
Bot API in - H	70.64	14.55	-	-	-	-	4.84	0.48	8.49	-	1.01

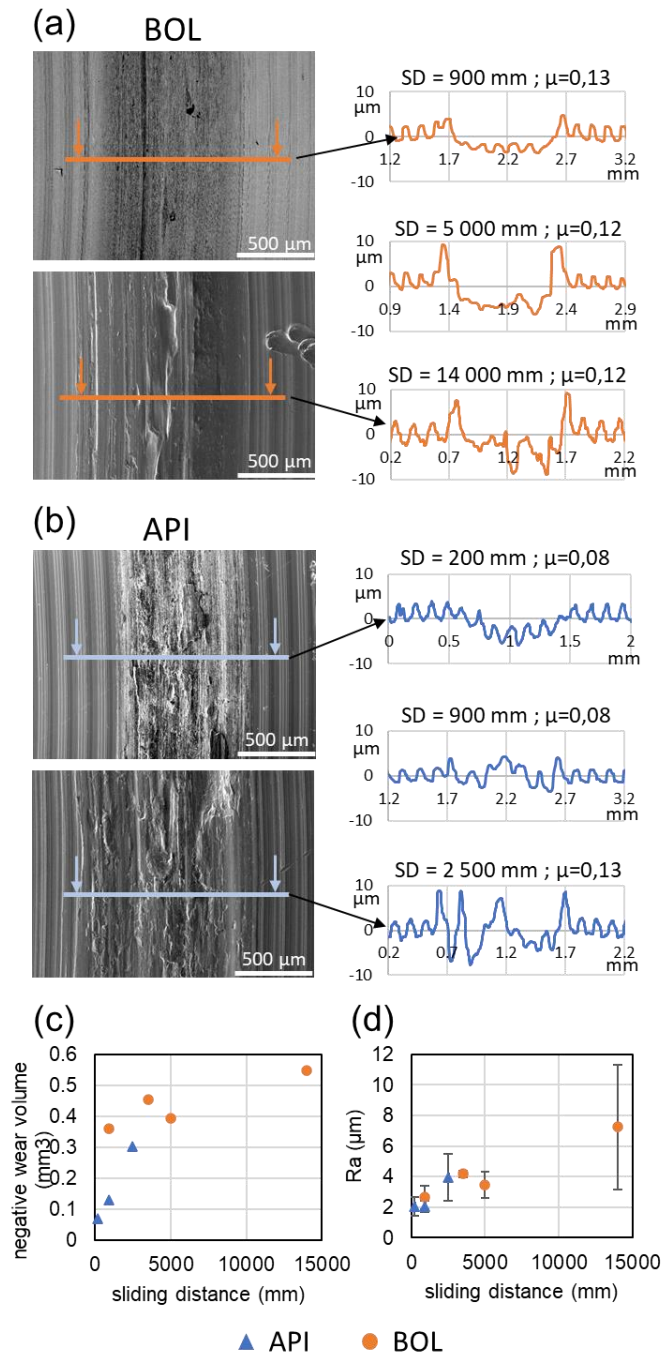


Figure 6 Evolution of the morphology of the wear tracks with the increase of sliding distance through SEM observations and line profiles for (a) BOL and (b) API, (c) and (d) evolution of respectively the negative wear volume and the roughness parameter Ra in the wear track on the bottom sample with the sliding distance ( $P_{\text{contact}} = 650 \text{ MPa}$ ,  $f = 0.4 \text{ Hz}$ ,  $\vartheta^* = \pm 25^\circ$ ,  $D = \pm 7.2 \text{ mm}$ )

**BOL** – On both specimens, out of the tracks, the XPS analyses reveal the presence of elements of grease (adsorbed on Mn-P layer or on steel). The carbon layer adsorbed on the surface is thinner than 10 nm for both samples since Mn-P layer and iron are detected by XPS. In the tracks of both top and bottom samples, elements of the Mn-P layer and the grease are detected by both EDS and XPS. Thus, Mn-P layer has transferred and a protective layer containing grease elements and manganese phosphate has been formed on both surfaces. On the top sample, the thickness of the worn Mn-P layer plus the protective layer is greater than 10 nm since no iron is detected by XPS but lower than few microns since EDS detects iron from the BOL bulk. Thickness of the bottom protective layer should be in the same range for the same reasons.

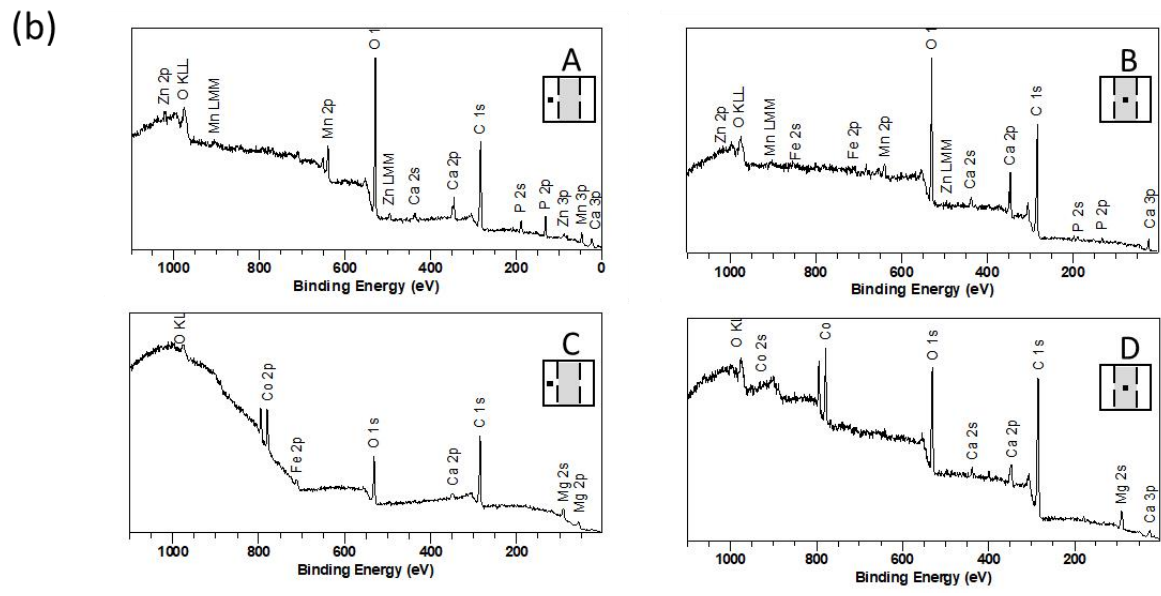
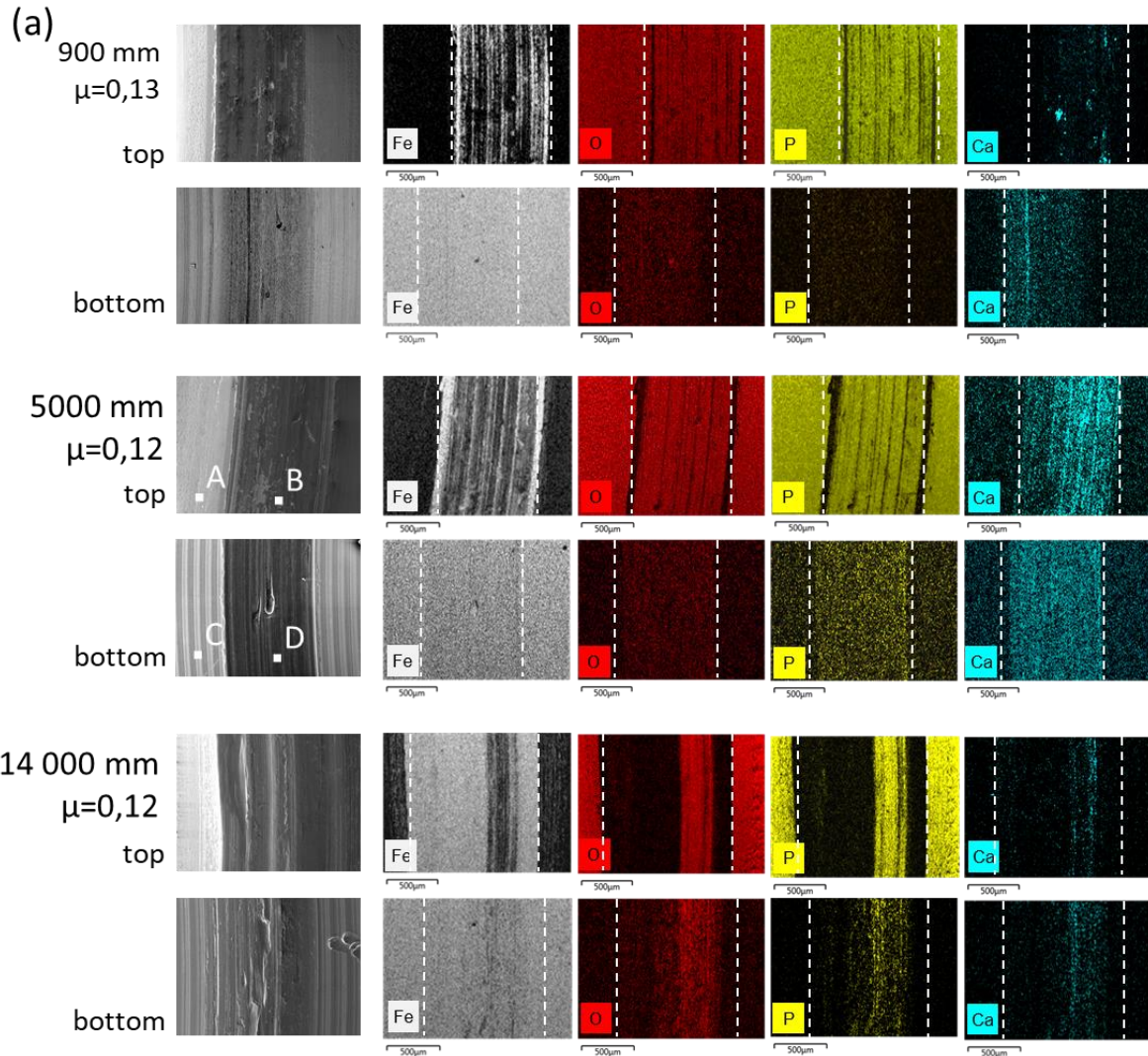


Figure 7 Surface analyses of the top and the bottom samples tested with BOL at 650 MPa for different sliding distances, (a) SEM observations and EDS analyses, (b) XPS spectra on samples rubbed until a sliding distance of 5000 mm, A : top - out of track, B top - middle of track, C - bottom out of track and D - bottom middle of track ( $P_{\text{contact}} = 650 \text{ MPa}$ ,  $f = 0.4 \text{ Hz}$ ,  $\vartheta^* = \pm 25^\circ$ ,  $D = \pm 7.2 \text{ mm}$ )



Table 6 Elements detected by EDS and XPS and their origin in the interface

Sample	EDS	XPS	Origin of elements
BOL top sample	C, Fe	Co	Steel
	Mn, O, P, Ca	O, P, Mn, Ca, Zn	Mn-P layer
	C, Ca	C, Ca, Mg	Grease
	C	C	Contamination
BOL bottom sample	Fe, O	Fe, O, C, Co	Steel
	P, Mn, O	P, Mn	Mn-P layer
	C, Ca	Ca, Mg	Grease
	C	C	Contamination
API top sample	Fe	Mn, P, O, Mg, Ca	Steel
	Mn, P, O	Mn, P, O, Mg, Ca	Mn-P layer
	Pb, C, Zn	C, Ca, Pb, Zn, Cu	Grease
		C	Contamination
API bottom sample	Fe, O, C	Fe, O, C, Co	Steel
	P, Mn, O		Mn-P layer
		Ca, Pb, Zn	Grease
		C	Contamination

*API* – On both specimens, XPS detected both elements of the grease (mainly lead) outside the tracks. Again, carbon layer adsorbed on the surface is thinner than 10 nm on the top and bottom samples out of the tracks since elements from Mn-P layer and steel are detected using XPS. Inside both tracks, iron is detected by EDS where there is neither Mn-P nor lead. On top sample, lead is in the form of small patches distributed in the track's width. On the bottom tracks, lead and phosphorus are quite well spread in the interface with lacks at some places. The third-body layer on the top sample is a mix between Mn-P layer and lead while third-body on the bottom sample is mainly composed of lead. Mn-P layer is transferred however it cannot be detected on the extreme surface by XPS. Both Pb-layers are thicker than some microns since no iron is detected in EDS where interfacial material is present.

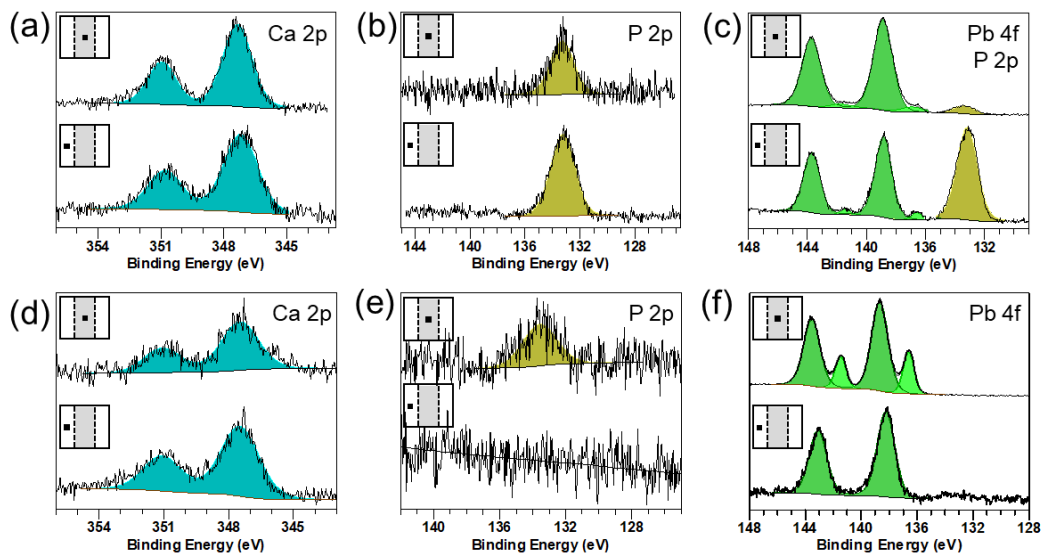


Figure 9 XPS high resolution spectra in and out of the tracks for BOL and API, (a) Ca 2p and (b) P 2p on BOL top sample, (d) Ca 2p and (e) P 2p on BOL bottom sample, (c) Pb4f and P 2p on API top sample, (d) Pb 4f on API bottom sample ( $P_{contact} = 650$  MPa,  $f = 0.4$  Hz,  $\vartheta^* = \pm 25^\circ$ ,  $D = \pm 7.2$  mm)

To better understand the composition of the protective layers, high resolution spectra were made and compared to the initial state of the surfaces for each sample. The spectra are shown in Figure 9 and the corresponding peaks fitting parameters are in Table 7 for BOL samples and Table 8 for API samples. The calcium, the lead and the

phosphorus were fitted as reference elements respectively of the BOL, the API and the Mn-P layer. First for BOL, by comparing analysis in the tracks and out, no chemical shift is found neither for the calcium nor for phosphorus on both surfaces. This suggests that particles of Mn-P are detached and mechanically mixed with the grease particles forming a thin interfacial layer. In case of API, on top sample, in and out of track, Pb displays two sets of doublet characteristic of two different chemical compounds. The first doublet at position 136.9 and 141.3 eV is a characteristic of 4f7/2 and 4f5/2 transitions in Pb metal while the second doublet, shifted towards higher binding energies (138.8 and 143,3 eV for Pb4f7/2 and Pb5f5/2 respectively) may be attributed to an oxide or a lead carbonate [22–24]. Proportion of lead increases in the track. On the bottom sample, the proportion of Pb metal increases in the track.

Table 7 XPS peaks assignation and elements proportion for BOL top and bottom samples

	Name	Position	FWHM	At%	Species	Ref.
Top sample						
in track	Ca 2p	347.36	1.64	72.30		
	P 2p	133,30	2.06	27.70	Phosphate	[20]
out of track	Ca 2p	347.20	1.94	29.57		
	P 2p	133.18	1.65	70.43	Phosphate	[20]
Bottom sample						
in track	Ca 2p	347.47	2.06	100		
out of track	Ca 2p	347.49	2.12	78.01		
	P 2p	133.18	1.65	21.99	Phosphate	[20]

Table 8 XPS peaks assignation and elements proportion for API top and bottom samples

	Name	Position	FWHM	At%	Species	Ref.
Top sample						
in track	Pb 4f	136.93	1.84	2.70	Pb metal	[25]
		138.85	1.33	38.15	Oxydes or carbonates	[22,24]
	P 2p	133.35	1.67	59.15	Phosphate	[20]
out of track	Pb 4	136.59	0.82	0.37	Pb metal	[25]
		138.85	1.33	6.57	Oxydes or carbonates	[22,24]
	P 2p	133.18	1.65	93.06	Phosphate	[20]
Bottom sample						
in track	Pb 4f	138.22	1.48	100	Oxydes or carbonates	[22,24]
out of track	Pb 4f	136.60	0.93	23.75	Pb metal	[25]
		138.67	1.40	76.25	Oxydes or carbonates	[22,24]

#### IV) Discussion

Results in friction and wear as well as top surface analyses provide wear mechanisms for BOL and API.

In case of BOL, particles of the Mn-P layer break and are released in the contact. Due to pressure and shear, these particles are mechanically mixed with the particles of the grease until a thin protective layer is formed. Ernens *et al.* also observed this type of layer when using Mn-P layer with a grease (which was not BOL in this case) [26]. Most of the wear is done at the beginning of the test during the layer formation. Then wear rate decreases as well as friction coefficient, this may be due to the better distribution of the grease all over the contact observed at the middle of the tests. The protective layer performances increase with the sliding distance and pressure. The protective layer is then ripped of allowing steel-steel contact and galling initiation. Then, galling propagates then quickly in few cycles.

In case of API, the mechanism is mainly governed by lead particles presence. Particles are squeezed in the contact and packed forming a thick third-body layer on the steel sample right after surfaces start sliding as seen on EDS observations. This phenomenon is confirmed by XPS analyses, the native oxide layer around Pb particles (responsible of the highest binding energy peaks) breaks as particles are flattened in the contact exposing Pb metal detected in the middle of the track. Nevsad *et al.* also observed a thick Pb-containing layer on the top of the Mn-P layer when using API modified [9]. The Pb layer acts as a soft protective lubricious metal film between two hard solids. The mechanism of solid lubrication is reported by Stachowiak and Batchelor [27]. The contact area of contact is determined by the hard substrate and the shear strength of the interface is determined by the softer and weaker metal. Frictional force determined by the product of asperity shear strength and the contact area become quite low. The protective layer is gradually removed from the contact until galling occurs and propagates quickly. In both cases, severe wear appears at the edge of the contact and propagates toward the center. It is explained by the fact that pressure is higher at the edge in a flat-on-flat contact. API protective layer is formed quickly and is more performant than the BOL one providing immediately a protective low shear layer. However, lead layer is less durable than the layer formed in the presence of Mn-P and BOL.

In industrial application, the sliding distances reach a maximum of one thousand of millimeters during one screwdriving-unscrewing phase of a connection. To capture the performances of the greases at such sliding distances, two criteria on the friction coefficient and negative wear volume at a sliding distance of 900 mm are introduced. Comparison is shown in Figure 10 Criteria of comparison of the greases BOL and API, friction coefficient and negative wear volume at a sliding distance of 900 mm. Using both criteria, API appears to have the best performances. Indeed, at this short sliding distance, API presents the lowest friction coefficient as well as the lowest wear volume. This is in accordance with the full-scale experiments where API modified greases are known to be the best performing one [21,28]. After one make-up/break-out of the connection, fresh grease is applied on surfaces before the next screwing phase. Hence, the most important effect of grease application is to provide an effective protective layer immediately after surfaces start to rub and this is better achieved by API. This suggests also that the usual long term test procedure consisting in identifying the Nc endurance value after a single grease application is not representative of the real application. It may induce a bad choice regarding the grease performance as illustrated in Figure 5 where the BOL lubricant was considered as the most enduring (i.e. longest Nc). To alleviate such misfitting, current developments are undertaken to allow more representative loading sequences. It consists in the application of the normal load followed by the application of a short sliding period. Then, contact is opened allowing the application of fresh grease in the contact. This block loading sequence will be automatically repeated until the contact fails to extrapolate representative contact endurance values. Using this new experimental test procedure, providing more representative tribological results, we expect to achieve optimized future surface treatments but also grease composition for the studied application.

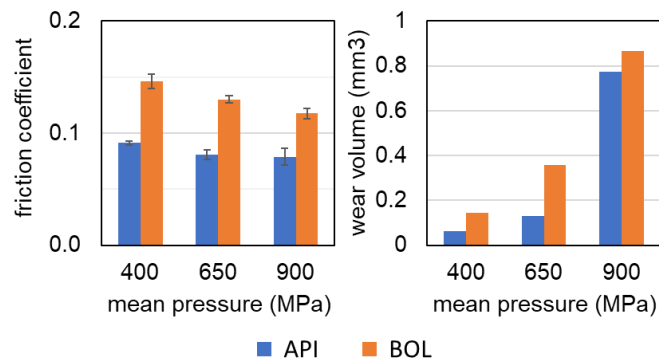


Figure 10 Criteria of comparison of the greases BOL and API, friction coefficient and negative wear volume at a sliding distance of 900 mm

## Conclusion

Two API 5A3 [21] greases have been compared using an original alternated ring-on-ring test system reproducing surface contact and pressure loading conditions found in OCTG premium connection during installation phase. The greases have been tested in a carbon steel interface implying manganese phosphate treatment on one side. Both greases have shown completely different mechanisms of lubrications and wear. Elements of Bestolife 4010NM® are mixed with detached particles of the manganese phosphate layer forming a long-lasting third body. Lead in API modified is acting as a soft metal film leading to solid lubrication. Protective layer formed with API reduces friction better than BOL layer does. For short sliding distances, the interface produces less wear using API than using BOL. Further understandings of protective layer's degradation and galling initiation in this type of interface should be done doing more interrupted tests and cross-section of the wear tracks. This investigation also underlines the necessity to reproduce more representative sliding and contact opening loading sequences including periodic lubrications to better illustrate the real OCTG tubes connection process.

## V) References

- [1] W.R. Blackstone, The development of a new test method for the evaluation of galling in OCTG connections, Thesis, Texas Tech University, 1987. <https://ttu-ir.tdl.org/handle/2346/12310> (accessed April 19, 2021).
- [2] C. Blanc, J. Lewis, A. Ichim, D. Mutis, A. Zestran, C.I. Lucca, L. Perello, New OCTG Developments to Overcome Challenges in Unconventional Plays, in: Day 2 Wed, October 16, 2019, SPE, Charleston, West Virginia, USA, 2019: p. D021S001R002. <https://doi.org/10.2118/196596-MS>.
- [3] O.G. Meza, S.. Sinaga, Overview of Lubrication Regimes and Contact Pressure Distribution in Proprietary Tubular Connections for Special Drilling Environments, in: Day 1 Mon, January 29, 2018, SPE, Abu Dhabi, UAE, 2018: p. D011S004R004. <https://doi.org/10.2118/189367-MS>.
- [4] G02 Committee, Test Method for Galling Resistance of Material Couples, ASTM International, 2021. <https://doi.org/10.1520/G0196-08R21>.
- [5] K.K. Kakulite, B. Kandasubramanian, Rudiment of 'galling: Tribological phenomenon' for engineering components in aggregate with the advancement in functioning of the anti-galling coatings, Surfaces and Interfaces. 17 (2019) 100383. <https://doi.org/10.1016/j.surfin.2019.100383>.
- [6] J. Perry, T.S. Eyre, The effect of phosphating on the friction and wear properties of grey cast iron, Wear. 43 (1977) 185–197. [https://doi.org/10.1016/0043-1648\(77\)90113-2](https://doi.org/10.1016/0043-1648(77)90113-2).
- [7] J. Zhang, H. Li, Influence of manganese phosphating on wear resistance of steel piston material under boundary lubrication condition, Surface and Coatings Technology. 304 (2016) 530–536. <https://doi.org/10.1016/j.surfcoat.2016.07.065>.
- [8] D.. Ernens, E.J. Riet, M.B. de Rooij, H.R. Pasaribu, W.M. van Haaften, D.J. Schipper, The Role of Phosphate Conversion Coatings in Make-Up of Casing Connections, in: Day 1 Tue, March 14, 2017, SPE, The Hague, The Netherlands, 2017: p. D011S005R001. <https://doi.org/10.2118/184690-MS>.
- [9] A. Nevesad, Tribological Interaction of Manganese Phosphate Coatings with Grease and Solid Lubricant Particles, Tribology Letters. (2020) 10.
- [10] L. Zang, Y. Chen, Y. Wu, Y. Zheng, H. Chen, D. You, L. Li, J. Li, Comparative tribological and friction behaviors of oil-lubricated manganese phosphate conversion coatings with different crystal sizes on AISI 52100 steel, Wear. 458–459 (2020) 203427. <https://doi.org/10.1016/j.wear.2020.203427>.

- [11] S.R. Hummel, J. Helm, Galling50, a Stochastic Measure of Galling Resistance, *Journal of Tribology*. 131 (2009). <https://doi.org/10.1115/1.3123344>.
- [12] A. Ertas, H.J. Carper, O. Cuvalci, S. Ekworo-Osire, W.R. Blackstone, Experimental Investigation of Galling Resistance in OCTG Connections, *Journal of Engineering for Industry*. 114 (1992) 100–104. <https://doi.org/10.1115/1.2899745>.
- [13] H.J. Carper, A. Ertas, J. Issa, O. Cuvalci, Effect of Some Material, Manufacturing, and Operating Variables on the Friction Coefficient in OCTG Connections, *Journal of Tribology*. 114 (1992) 698–705. <https://doi.org/10.1115/1.2920938>.
- [14] O. Cuvalci, H. Sofuoglu, A. Ertas, Effect of surface coating and tin plating on friction characteristics of P-110 tubing for different thread compounds, *Tribology International*. 36 (2003) 757–764. [https://doi.org/10.1016/S0301-679X\(03\)00057-4](https://doi.org/10.1016/S0301-679X(03)00057-4).
- [15] P. Faura, S. Fouvry, P. Ronfard, N. Marouf, T. Mathon, An experimental investigation of galling phenomenon generated in an alternated sliding ring-on-ring interface: Application to a full-scale solid lubricant interface, *Wear*. 508–509 (2022) 204457. <https://doi.org/10.1016/j.wear.2022.204457>.
- [16] C.D. Wagner, L.E. Davis, M.V. Zeller, J.A. Taylor, R.H. Raymond, L.H. Gale, Empirical atomic sensitivity factors for quantitative analysis by electron spectroscopy for chemical analysis, *Surface and Interface Analysis*. 3 (1981) 211–225. <https://doi.org/10.1002/sia.740030506>.
- [17] API Specification 5CT, Casing and tubing, API, 2021. <https://www.api.org/>.
- [18] K. Chiba, R. Ohmori, H. Tanigawa, T. Yoneoka, S. Tanaka, H<sub>2</sub>O trapping on various materials studied by AFM and XPS, *Fusion Engineering and Design*. 49–50 (2000) 791–797. [https://doi.org/10.1016/S0920-3796\(00\)00187-3](https://doi.org/10.1016/S0920-3796(00)00187-3).
- [19] X. Cai, L. Shi, W. Sun, H. Zhao, H. Li, H. He, M. Lan, A facile way to fabricate manganese phosphate self-assembled carbon networks as efficient electrochemical catalysts for real-time monitoring of superoxide anions released from HepG2 cells, *Biosensors and Bioelectronics*. 102 (2018) 171–178. <https://doi.org/10.1016/j.bios.2017.11.020>.
- [20] L. Guo, Q. Huang, C. Zhang, J. Wang, G. Shen, C. Ban, L. Guo, Study on the formation of Mn-P coatings with significant corrosion resistance on Q235 carbon steels by adjusting the ratio of phosphorus to manganese, *Corrosion Science*. 178 (2021) 108960. <https://doi.org/10.1016/j.corsci.2020.108960>.
- [21] API RP 5A3 : Recommended Practice on Thread Compounds for Casing, Tubing, Line Pipe, and Drill Stem Elements, (n.d.). [https://global.ihp.com/doc\\_detail.cfm?&input\\_search\\_filter=API&item\\_s\\_key=00237622&item\\_key\\_date=781131&input\\_doc\\_number=5A3&input\\_doc\\_title=&org\\_code=API](https://global.ihp.com/doc_detail.cfm?&input_search_filter=API&item_s_key=00237622&item_key_date=781131&input_doc_number=5A3&input_doc_title=&org_code=API) (accessed December 17, 2021).
- [22] P.W. Wang, L. Zhang, Structural role of lead in lead silicate glasses derived from XPS spectra, *Journal of Non-Crystalline Solids*. 194 (1996) 129–134. [https://doi.org/10.1016/0022-3093\(95\)00471-8](https://doi.org/10.1016/0022-3093(95)00471-8).
- [23] K. Laajalehto, R.St.C. Smart, J. Ralston, E. Suoninen, STM and XPS investigation of reaction of galena in air, *Applied Surface Science*. 64 (1993) 29–39. [https://doi.org/10.1016/0169-4332\(93\)90019-8](https://doi.org/10.1016/0169-4332(93)90019-8).
- [24] C. Powell, X-ray Photoelectron Spectroscopy Database XPS, Version 4.1, NIST Standard Reference Database 20, (1989). <https://doi.org/10.18434/T4T88K>.
- [25] D. Briggs, Handbook of X-ray Photoelectron Spectroscopy C. D. Wanger, W. M. Riggs, L. E. Davis, J. F. Moulder and G. E. Muilenberg Perkin-Elmer Corp., Physical Electronics Division, Eden Prairie, Minnesota, USA, 1979. 190 pp. \$195, *Surface and Interface Analysis*. 3 (1981) v–v. <https://doi.org/10.1002/sia.740030412>.
- [26] D. Ernens, G. Langedijk, P. Smit, M.B. de Rooij, H.R. Pasaribu, D.J. Schipper, Characterization of the Adsorption Mechanism of Manganese Phosphate Conversion Coating Derived Tribofilms, *Tribol Lett*. 66 (2018) 131. <https://doi.org/10.1007/s11249-018-1082-2>.
- [27] G.W. Stachowiak, A.W. Batchelor, Solid lubrication and surface treatments, in: *Engineering Tribology*, Butterworth-Heinemann, 2013.
- [28] E. Scavo, Design of an Environmentally Benign Thread Compound for Oil Well Joints, (2018) 110.